

February 7, 2022

Muon g-2 and LHC phenomenology in the $L_\mu - L_\tau$ gauge symmetric model

Keisuke Harigaya¹, Takafumi Igari², Mihoko M. Nojiri^{3,1},
Michihisa Takeuchi⁴, and Kazuhiro Tobe^{2,5}

¹*Kavli IPMU (WPI), TODIAS, University of Tokyo, Chiba, Kashiwa, 277-8583, Japan*

²*Department of Physics, Nagoya University, Aichi, Nagoya 464-8602, Japan*

³*Theory Center, KEK, Tsukuba, Ibaraki 305-0801, Japan*

⁴*Theoretical Particle Physics and Cosmology Group, Department of Physics, King's College
London, London WC2R 2LS, UK*

⁵*Kobayashi-Maskawa Institute for the Origin of Particles and the Universe,
Nagoya University, Aichi, Nagoya 464-8602, Japan*

Abstract

In this paper, we consider phenomenology of a model with an $L_\mu - L_\tau$ gauge symmetry. Since the muon couples to the $L_\mu - L_\tau$ gauge boson (called Z'' boson), its contribution to the muon anomalous magnetic moment (muon g-2) can account for the discrepancy between the standard model prediction and the experimental measurements. On the other hand, the Z'' boson does not interact with the electron and quarks, and hence there are no strong constraints from collider experiments even if the Z'' boson mass is of the order of the electroweak scale. We show an allowed region of a parameter space in the $L_\mu - L_\tau$ symmetric model, taking into account consistency with the electroweak precision measurements as well as the muon g-2. We study the Large Hadron Collider (LHC) phenomenology, and show that the current and future data would probe the interesting parameter space for this model.

KCL-PH-TH/2013-37

KEK-TH-1684

IPMU 13-0213

1 Introduction

The Standard Model of elementary particles (SM) has been very successful in describing the nature at the electroweak (EW) scale. Recently, the ATLAS and CMS collaborations at the Large Hadron Collider (LHC) have discovered a new particle [1, 2], which is consistent with the SM Higgs boson. This discovery also strengthens the correctness of the SM. So far, no explicit evidence of physics beyond the SM has been reported from the LHC.

Several groups, however, have reported an anomaly of the muon anomalous magnetic moment $a_\mu = (g-2)/2$ (muon g-2), which has been precisely measured experimentally [3] and compared with state-of-the-art theoretical predictions (for example, see [4, 5, 6, 7, 8, 9, 10, 11] and references therein). The estimated discrepancies between the SM predictions and the measured value are consistently more than 3σ , as listed in Table 1.

Although it is too early to conclude that this anomaly is evidence of new physics beyond the SM, we expect new particles and interactions related with the muon sector once we regard it as a hint of new physics. Gauge interactions have been playing a central role to construct fundamental models in particle physics history. Following this line, in this paper, we pursue the possibility that the muon has a new gauge interaction beyond the SM*.

$a_\mu^{\text{Exp}} [10^{-10}]$	$\delta a_\mu = a_\mu^{\text{Exp}} - a_\mu^{\text{SM}} [10^{-10}]$
11659208.9 ± 6.3	$26.1 \pm 8.0 (3.3\sigma) [6]$
	$31.6 \pm 7.9 (4.0\sigma) [7]$
	$33.5 \pm 8.2 (4.1\sigma) [8]$
	$28.3 \pm 8.7 (3.3\sigma) [9]$
	$29.0 \pm 9.0 (3.2\sigma) [10]$
	$28.7 \pm 8.0 (3.6\sigma) [11]$

Table 1: Measured muon g-2 (a_μ^{Exp}) and the estimated differences (δa_μ) from the recent SM predictions in several references.

The discrepancy is of the same order as the contribution from the EW gauge bosons W^\pm and Z , $a_\mu^{\text{EW}} = (15.4 \pm 0.2) \times 10^{-10}$ [5]. Assuming the anomaly is due to the quantum effects of the new particles, this discrepancy suggests that their masses should be at the EW scale, which is well within the reach of the LHC. Thus, it is very interesting to study the phenomenology at the LHC.

The coupling of the new light gauge bosons to the electron and light quarks are severely constrained by the LEP [14, 15], Tevatron [16, 17] and LHC [18, 19]. Therefore, if the new gauge interaction is the flavor universal one such as the $B-L$ gauge interaction, the gauge coupling has to be small and hence the new gauge boson has to be very light as well in order to induce enough contributions to the muon g-2. An explicit model of this category is the

* If the new interaction is Yukawa-type one, new fermion or/and new scalar will be introduced. A well-known example of this category is the minimal supersymmetric model [12]. Other models have been also discussed in Refs. [13].

hidden photon model [20, 21], and constraints on the hidden photon model have been studied in detail [22, 23].

Another possibility is a flavor-dependent gauge interaction. If the gauge boson couples to the muon but not to the electron nor quarks, the gauge interaction can explain muon g-2 while keeping the consistency with the direct search results. A simple candidate is based on anomaly free $L_\mu - L_\tau$ gauge symmetry [24, 25, 26, 27, 28], where L_μ and L_τ are μ and τ lepton numbers, respectively. We consider this model in detail. In addition to the SM particles, this model has one extra gauge boson associated to the $L_\mu - L_\tau$ gauge symmetry, which we refer to as a Z'' boson. Note that only the 2nd and the 3rd generation leptons couple to the Z'' gauge boson, and hence the constraints from the direct search experiments are very weak.

Organization of this paper is the following. In the next section, we introduce a model with the $L_\mu - L_\tau$ gauge symmetry, which we refer to as a Z'' model. In section 3, we study the parameter space of the Z'' model where the anomaly of the muon g-2 can be explained. Since the mass of the Z'' gauge boson is expected to be of the EW scale if the gauge coupling is of order unity, the Z'' boson affects the EW precision observables. We investigate the effects and show the parameter space consistent with the data. In section 4, we study the LHC phenomenology. We show that the 4μ channel as well as the $2\mu 2\tau$ channel are effective for the Z'' boson search. In section 5, we summarize our results.

2 Z'' model

The differences between two lepton-flavor numbers $L_i - L_j$ ($i \neq j$), where L_i are lepton-flavor numbers, $L_i = (L_e, L_\mu, L_\tau)$, are anomaly free in the SM. Therefore, the SM gauge symmetry (G_{SM}) can be extended to $G_{\text{SM}} \times U(1)_{L_i - L_j}$ without the addition of any exotic fermions, and such extensions are one of the minimal and economical $U(1)$ extensions of the SM.

In particular, the $L_\mu - L_\tau$ gauge symmetry is attractive because it solves a problem of the muon g-2 without contradictions to other experiments. The gauge boson, called Z'' boson, couples to the 2nd and 3rd generation leptons, so that it provides an extra contribution to the muon g-2. Since the Z'' boson does not couple to the electron nor any quarks, it avoids the strong constraints from the direct search experiments.

In this paper, we consider a model based on $G_{\text{SM}} \times U(1)_{L_\mu - L_\tau}$. The interactions of the Z'' boson are given by

$$\mathcal{L}_{\text{int}} = -g_{Z''} Z''_\mu \sum_{f=\mu, \tau, \nu_\mu, \nu_\tau} Q_f'' \bar{f} \gamma^\mu f, \quad (2.1)$$

where Q_f'' is a $U(1)_{L_\mu - L_\tau}$ charge of a fermion f as shown in Table 2, and $g_{Z''}$ is the gauge coupling constant of the $U(1)_{L_\mu - L_\tau}$ gauge symmetry. We assume that the $L_\mu - L_\tau$ gauge symmetry is spontaneously broken and the Z'' boson becomes massive. The gauge coupling $g_{Z''}$ and the Z'' mass $m_{Z''}$ are the only free parameters in this model.

Right-handed neutrinos $\nu_{\ell R}$ ($\ell = \mu, \tau$) can be light or heavy, depending on the model of neutrino masses in this framework. If they are light enough such that the decay mode $Z'' \rightarrow$

particle	$L_2 = (\nu_{\mu L}, \mu_L)$	$L_3 = (\nu_{\tau L}, \tau_L)$	$(\mu_R)^c$	$(\tau_R)^c$	$(\nu_{\mu R})^c$	$(\nu_{\tau R})^c$	others
charge	+1	-1	-1	+1	-1	+1	0

Table 2: Charges under the $L_\mu - L_\tau$ gauge symmetry. All fields are in left-handed basis.

$\nu_{\ell R} \bar{\nu}_{\ell R}$ is open, the branching ratio $BR(Z'' \rightarrow \mu^+ \mu^- / \tau^+ \tau^-)$ is about 1/4, respectively. On the other hand, if they are heavy enough, $BR(Z'' \rightarrow \mu^+ \mu^- / \tau^+ \tau^-)$ is about 1/3, respectively. Because of the smaller $\mu^+ \mu^- / \tau^+ \tau^-$ branching ratio, it is more difficult to observe the Z'' boson signal in the case that the right-handed neutrinos are light. In order to be conservative, we assume that the right-handed neutrinos are light enough, and we refer to the model with this assumption as a Z'' model. We discuss a model with the correct neutrino masses and mixings in Appendix A.

In general, the Z'' gauge boson can mix with the Z boson and photon since the $L_\mu - L_\tau$ symmetry is a $U(1)$ gauge symmetry. Such mixings are naturally suppressed if the $L_\mu - L_\tau$ gauge symmetry is embedded into a non-Abelian symmetry at the more fundamental level [27]. Therefore, in this paper, we assume that the $U(1)$ mixing effect is negligible.

3 Muon g-2 and electroweak precision observables

In this section, we study the parameter space of the Z'' model in which the measured muon g-2 is explained while satisfying the constraints from the EW precision observables. As shown in Table 2, the Z'' gauge boson interacts with the muon through the $L_\mu - L_\tau$ gauge interaction. The new contribution to the muon g-2 (δa_μ) is induced through a Feynman diagram depicted in Figure 1, and it is given by the following expression [26],

$$\delta a_\mu = \frac{g_{Z''}^2}{12\pi^2} \frac{m_\mu^2}{m_{Z''}^2} \simeq 2 \times 10^{-9} \left(\frac{g_{Z''}}{0.5} \right)^2 \left(\frac{100 \text{ GeV}}{m_{Z''}} \right)^2. \quad (3.2)$$

Here, we have assumed that $m_{Z''} \gg m_\mu$. Figure 2 shows the dependence of δa_μ on the two model parameters. It can be seen that the effect of the Z'' boson with $g_{Z''} = O(1)$ and $m_{Z''} = O(100)$ GeV compensates the 3σ deviation observed in the muon g-2 measurement.

Since Z'' couples to the 2nd and 3rd generation leptons (l, ν_l), it induces extra contributions to $Z\bar{l}l$ and $W^+ l^- \bar{\nu}_l$ vertices. The Z'' boson effects appear on the EW precision observables through these vertex corrections. The effective vertex $Z_\mu \bar{f} f$ is given by

$$\frac{ig}{c_W} \gamma_\mu (g_L^f P_L + g_R^f P_R), \quad (3.3)$$

where

$$g_L^f = (T_f^3 - Q_f s_W^2)(1 + \Delta), \quad g_R^f = -Q_f s_W^2(1 + \Delta). \quad (3.4)$$

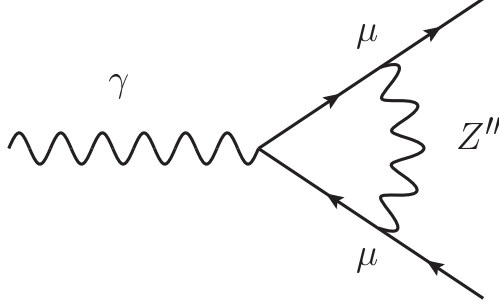


Figure 1: Feynman diagram for muon g-2, mediated by the Z'' gauge boson.

Note that one-loop corrections are parametrized by Δ , which is independent of f ($f = \mu, \tau, \nu_\mu, \nu_\tau$) if the lepton masses are neglected. Δ is given by [29]

$$\Delta = \Delta^{(1)} + \delta Z, \quad (3.5)$$

$$\Delta^{(1)} = -\frac{g_{Z''}^2}{8\pi^2} \text{Re} [q^2 \{C_0 + C_{11} + C_{23} - C_{22}\} - 2(1 - \epsilon)^2 C_{24}] (Z'', \mu, \mu; p, q), \quad (3.6)$$

$$\delta Z = -\frac{g_{Z''}^2}{8\pi^2} (1 - \epsilon) (B_0 + B_1) (Z'', \mu; p^2 = m_\mu^2), \quad (3.7)$$

where $\Delta^{(1)}$ is an one-loop vertex correction and δZ is a counter term contribution from the wave function renormalization of the leptons. p and q are external momenta of the muon

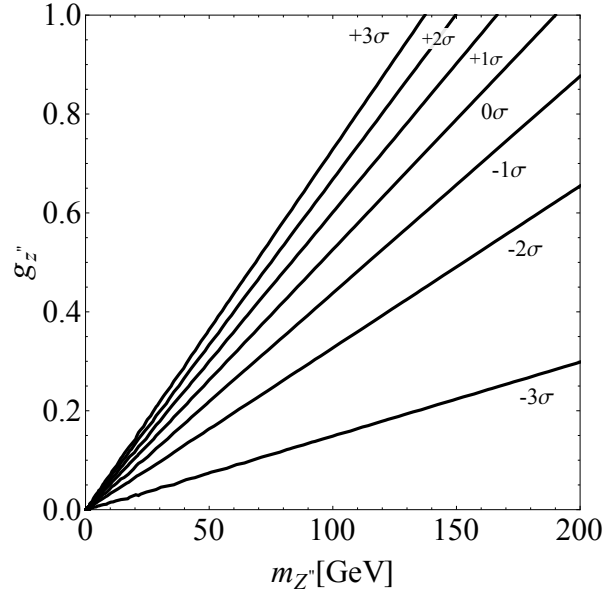


Figure 2: Contours of the standard deviations for muon g-2 with the Z'' contribution (δa_μ) in $(m_{Z''}, g_{Z''})$ plane.

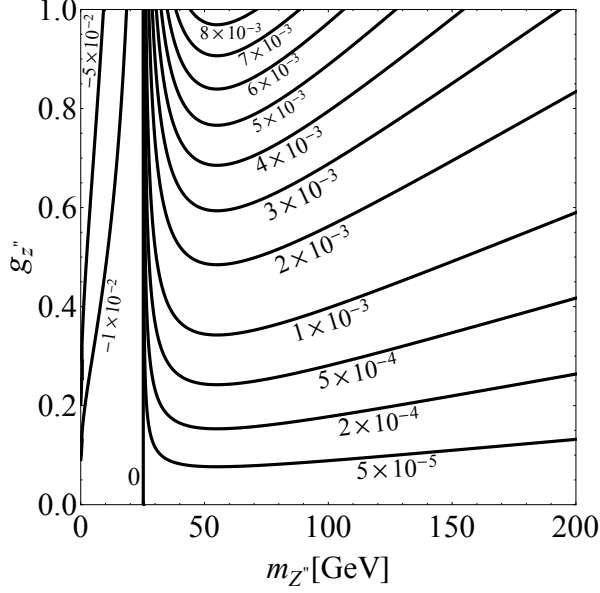


Figure 3: The vertex correction Δ at the Z -pole ($q^2 = m_Z^2$) is shown as a function of $m_{Z''}$ and $g_{Z''}$.

and the Z boson, respectively. C_{XX} and B_X , so-called the Passarino-Veltman functions, are given in Appendix B. The explicit form of Δ is

$$\begin{aligned} \Delta(q^2) = & -\frac{g_{Z''}^2}{8\pi^2} \left[\frac{7}{4} + \delta + \left(\delta + \frac{3}{2} \right) \log \delta \right. \\ & \left. + (1 + \delta)^2 \left\{ \text{Li}_2 \left(\frac{\delta}{1 + \delta} \right) + \frac{1}{2} \log^2 \left(\frac{\delta}{1 + \delta} \right) - \frac{\pi^2}{6} \right\} \right], \end{aligned} \quad (3.8)$$

where $\delta \equiv \frac{m_{Z''}^2}{q^2}$ and $\text{Li}_2(x) \equiv -\int_0^x dt \frac{\log(1-t)}{t}$ is the Spence function. Here, we have neglected the muon mass.

Figure 3 shows the numerical values of the vertex correction at the Z -pole $\Delta(q^2 = m_Z^2)$ as a function of $m_{Z''}$ and $g_{Z''}$. For example, with $g_{Z''} = 0.3$ and $m_{Z''} = 60$ GeV ($m_{Z''} = 80$ GeV), we obtain $\Delta(m_Z^2) = 7.6 \times 10^{-4}$ (6.7×10^{-4}).

Similarly, we can calculate an one loop correction to $W^+ l^- \bar{\nu}_l$ vertex ($l = \mu, \tau$) via the Z'' gauge boson, and the effective vertex is given by

$$\frac{ig}{\sqrt{2}} \gamma_\mu k_L^l P_L, \quad (3.9)$$

where

$$k_L^l = 1 + \Delta_W. \quad (3.10)$$

We obtain $\Delta_W = \Delta$ by neglecting the μ (τ) and ν_μ (ν_τ) masses.

One may be worried that the Z'' boson contribution to $W\mu\nu_\mu$ vertex may affect the muon decay, $\mu \rightarrow e\nu_\mu\bar{\nu}_e$. However, the momentum transfer of the virtual W boson is negligible in the muon decay compared to the mass scale of the Z'' boson. Therefore, the effect of the Z'' boson decouples in the muon decay.

We calculate the EW precision observables listed in Table 3. We adopt formulas in, for example, Refs. [30, 31, 32] for the calculation. We perform a χ^2 fit by varying input parameters m_t , m_h , $\Delta\alpha_{\text{had}}^{(5)}$ and α_s , in order to identify the parameter region consistent with the data. The χ^2 is defined by

$$\chi^2 = \sum_{i,j} \left(\frac{O_i^{\text{Exp}} - O_i^{\text{Model}}}{\sigma_i^{\text{Exp}}} \right)^2 (\rho^{-1})_{ij} \left(\frac{O_j^{\text{Exp}} - O_j^{\text{Model}}}{\sigma_j^{\text{Exp}}} \right)^2, \quad (3.11)$$

where O^{Exp} , σ^{Exp} and ρ are the measured value, the 1σ error and the correlation coefficient matrix of the observables, respectively, taken from Refs. [3, 6, 33], and O^{Model} is the theoretical prediction. In Table 3, we show the result at the best fit point for the SM and the results at the sample points with $m_{Z''} = (60, 80)$ GeV and $g_{Z''} = 0.3$ for the Z'' model.

The Z'' effects increase the partial Z decay widths of $l\bar{l}$ mode Γ_{ll} ($l = \mu, \tau, \nu_\mu$ and ν_τ) in the interesting parameter region while the Z total decay width Γ_Z does not increase significantly since the hadronic contributions Γ_{had} are dominant. Similarly, the effect on the W total decay width is also negligible. On the other hand, the effects on $\sigma_h^0 = \frac{12\pi}{m_Z^2} \frac{\Gamma_{ee}\Gamma_{\text{had}}}{\Gamma_Z^2}$ and $R_\mu = \frac{\Gamma_{\text{had}}}{\Gamma_{\mu\mu}}$ can be significant. As shown in Table 3, the observed value of σ_h^0 tends to be larger than the SM value. Adding Z'' contribution results in worse fittings. Similarly, since the observed value of R_μ is larger than the SM fitted value, adding the Z'' contribution makes the fit further worse.[†] As a result, large vertex corrections from the Z'' boson are disfavored.

In Figure 4, we show χ^2 of the Z'' model as a function of $m_{Z''}$ and $g_{Z''}$. As can be seen from the figure, small gauge coupling $g_{Z''} < 0.4$ and relatively light Z'' boson $m_{Z''} < 100$ GeV are favored.

[†] We also note that the Z'' contribution does not affect the left-right asymmetry $A_{\mu,\tau}$, because the Z'' universally contributes to the left- and right-handed μ and τ .

	data	SM fit	pull	Z'' model	pull	Z'' model	pull
Γ_Z (GeV)	2.4952(23)	2.4953	-0.06	2.4961	-0.4	2.4960	-0.3
σ_h^0 (nb)	41.541(37)	41.480	1.7	41.454	2.3	41.457	2.3
R_e	20.804(50)	20.739	1.3	20.739	1.3	20.739	1.3
R_μ	20.785(33)	20.739	1.4	20.708	2.3	20.712	2.2
R_τ	20.764(45)	20.787	-0.5	20.755	0.2	20.759	0.1
$A_{\text{FB}}^{0,e}$	0.0145(25)	0.0162	-0.7	0.0162	-0.7	0.0162	-0.7
$A_{\text{FB}}^{0,\mu}$	0.0169(13)	0.0162	0.5	0.0162	0.5	0.0162	0.5
$A_{\text{FB}}^{0,\tau}$	0.0188(17)	0.0162	1.5	0.0162	1.5	0.0162	1.5
τ pol.:							
A_τ	0.1439(43)	0.1472	-0.8	0.1472	-0.8	0.1472	-0.8
A_e	0.1498(49)	0.1472	0.5	0.1472	0.5	0.1472	0.5
b, c quarks:							
R_b	0.21629(66)	0.21579	0.8	0.21579	0.8	0.21578	0.8
R_c	0.1721(30)	0.1722	-0.05	0.1722	-0.05	0.1722	-0.05
$A_{\text{FB}}^{0,b}$	0.0992(16)	0.1032	-2.5	0.1032	-2.5	0.1032	-2.5
$A_{\text{FB}}^{0,c}$	0.0707(35)	0.0737	-0.9	0.0737	-0.9	0.0737	-0.9
A_b	0.923(20)	0.935	-0.6	0.935	-0.6	0.935	-0.6
A_c	0.670(27)	0.668	0.08	0.668	0.08	0.668	0.08
SLD:							
A_e	0.1516(21)	0.1472	2.1	0.1472	2.1	0.1472	2.1
A_μ	0.142(15)	0.1472	-0.3	0.1472	-0.3	0.1472	-0.3
A_τ	0.136(15)	0.1472	-0.7	0.1472	-0.7	0.1472	-0.7
W boson:							
M_W (GeV)	80.385(15)	80.362	1.5	80.362	1.5	80.362	1.5
Γ_W (GeV)	2.085(42)	2.091	-0.1	2.091	-0.2	2.091	-0.2
muon g-2:							
$\delta a_\mu (10^{-9})$	2.61(0.80)	0	3.3	2.36	1.1	1.33	1.1
Inputs							
$\Delta\alpha_{\text{had}}^{(5)}(M_Z^2)$	0.02763(14)	0.02760	0.2	0.02760	0.2	0.027560	0.2
$\alpha_s(M_Z)$	0.1184(7)	0.1184	0.0	0.1184	0.0	0.1184	0.0
m_t (GeV)	173.1(0.9)	173.7	-0.6	173.7	-0.6	173.7	-0.6
m_h (GeV)	125.9 (0.4)	125.9	0	125.9	0	125.9	0
$m_{Z''}$ (GeV)	-	-	-	60	-	80	-
$g_{Z''}$	-	-	-	0.3	-	0.3	-
$\chi^2/(d.o.f)$		35.1/(22)		29.2/(22)		31.0/(22)	

Table 3: The EW precision data and theoretical predictions of EW precision observables. The experimental data are taken from Ref. [33] except that M_W , Γ_W , m_t and m_h are from Ref. [3], and δa_μ and $\Delta\alpha_{\text{had}}^{(5)}$ are from Ref. [6]. The best fit values of the SM and sample points for Z'' model, $m_{Z''} = (60, 80)$ GeV and $g_{Z''} = 0.3$ are shown.

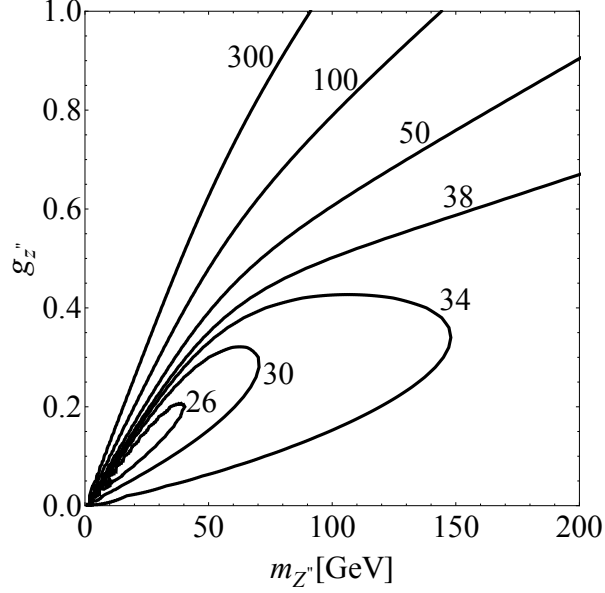


Figure 4: The total χ^2 in the $(m_{Z''}, g_{Z''})$ plane.

4 LHC phenomenology

In this section, we study the phenomenology of the Z'' model at the LHC and investigate whether the current and future LHC results can constrain or discover the Z'' boson in the region which is favored by the EW precision measurement as well as the muon g-2 shown in the previous section.

Relatively light Z'' bosons can be produced at e^+e^- , $p\bar{p}$ and pp collisions. The event including the decay is typically described by the diagram depicted in Figure 5.

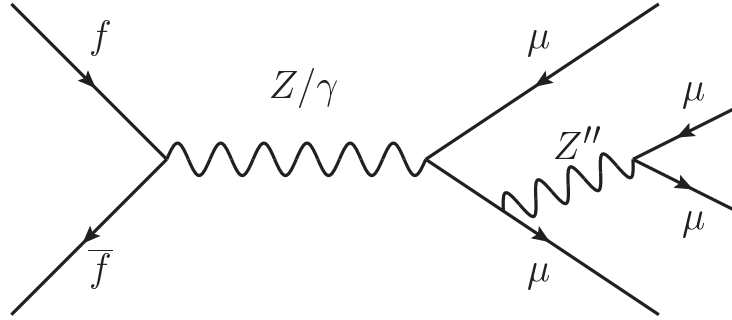


Figure 5: Feynman diagram for a typical Z'' boson production process at the tree-level.

Since the Z'' boson only couples to μ , τ , ν_μ and ν_τ , its effects only appear in the specific final states. Table 4 lists the final states where the Z'' boson contributes. In particular, the 4 lepton modes involving e^\pm are not affected.

final state	Z'' effects
$4\mu, 4\tau, 2\mu 2\tau, 2\mu + E_{T,\text{miss}}, 2\tau + E_{T,\text{miss}}$	yes
$4e, 2e2\mu, 2e2\tau, 2e + E_{T,\text{miss}}$	no

Table 4: List of 4 lepton final state processes relevant to the Z'' boson effects. Missing transverse energy, $E_{T,\text{miss}}$, is originated from neutrinos.

Table 5 lists the cross sections of typical processes for the SM and Z'' model for $m_{Z''} = 80$ GeV. The gauge coupling is fixed as $g_{Z''} = 0.3$ throughout this section unless otherwise stated. We see that there are no constraint we can set on the Z'' model from the LEP[‡] nor from the Tevatron due to the small cross sections. On the other hand, 4 μ final states have been already observed at 7-8 TeV LHC with $\int dtL = 25 \text{ fb}^{-1}$, and a few fb difference in the cross section would be or become measurable [26]. For the $2\mu 2\tau$ mode, it is difficult to constrain the Z'' model from the current data due to low τ identification efficiency though it would be possible with $\int dtL = 300 - 3000 \text{ fb}^{-1}$ at $\sqrt{s} = 14$ TeV.

In this section the results based on four signal samples with $m_{Z''} = 60, 80, 90$, and 100 GeV are shown. Note that the generated signals also include the SM and the interference contributions. We perform a parton level calculation using Calcchep-3.4 [34] and interface the events to Pythia-6.4.25 [35]. The detector effect is simulated with Delphes-2.0.5 [36].

process		cross section [fb]	
		SM	Z'' model ($m_{Z''} = 80$ GeV)
LEP ($\sqrt{s} = 200$ GeV)	$e^+e^- \rightarrow 4\mu$	3.8	3.8
Tevatron ($\sqrt{s} = 1.96$ TeV)	$p\bar{p} \rightarrow 4\mu$	3.4	3.6
LHC ($\sqrt{s} = 8$ TeV)	$pp \rightarrow 4\mu$	14	15
	$pp \rightarrow 2\mu 2\tau$	29	30
LHC ($\sqrt{s} = 14$ TeV)	$pp \rightarrow 4\mu$	27	28
	$pp \rightarrow 2\mu 2\tau$	57	59

Table 5: Cross sections in typical processes where the Z'' boson contributes, where $p_{T,l} > 5$ GeV and $m_{l-l^+} > 5$ GeV ($l = \mu$ and τ) are required. The numbers for the Z'' model are for $m_{Z''} = 80$ GeV and $g_{Z''} = 0.3$.

4.1 4 lepton channels at $\sqrt{s} = 7 - 8$ TeV

Both CMS [37] and ATLAS [38] collaborations have reported the measurements of Z decays to four leptons at $\sqrt{s} = 7$ and 8 TeV. Their measurements would be sensitive to the light Z'' boson. First, we consider how strongly the existence of the Z'' boson is constrained by the

[‡]In Ref. [26], authors discussed the LEP bound, however, we found their limit is too optimistic.

ATLAS data [§]. In the ATLAS analysis [38], they search for the production of four leptons: $e^+e^-e^+e^-$ ($4e$), $\mu^+\mu^-\mu^+\mu^-$ (4μ) and $e^+e^-\mu^+\mu^-$ ($2e2\mu$) at the Z resonance. We summarize the set of selection cuts they have used as follows:

1. four isolated leptons, which have two opposite sign and same-flavor di-lepton pairs, where $p_{T,\mu} > 4$ GeV and $|\eta_\mu| < 2.7$ ($p_{T,e} > 7$ GeV and $|\eta_e| < 2.47$).
2. the leading three leptons must have $p_{T,\ell} > 20, 15$, and 8 GeV, and if the third (p_T -ordered) lepton is an electron it must have $p_{T,e_3} > 10$ GeV.
3. the four leptons are required to be separated as $\Delta R_{\ell\ell} > 0.1$.
4. the invariant masses of the same-flavor and opposite-sign leptons are required to have $m_{l+l-} > 5$ GeV.
5. $m_{12} > 20$ GeV and $m_{34} > 5$ GeV, where m_{12} is the invariant mass of the same flavor and opposite sign di-lepton pair which is the closest to the Z boson mass among the possible combinations, while the other one is called m_{34} .
6. the invariant mass of the four leptons is in the m_Z window, $80 \text{ GeV} < m_{4l} < 100 \text{ GeV}$.

[§] The CMS has similar analysis in Ref. [37] and their result, however, is based on data collected at $\sqrt{s} = 7$ TeV. On the other hand, the ATLAS result is based on much larger set of data with integrated luminosities of 4.6 fb^{-1} at $\sqrt{s} = 7$ TeV and 20.7 fb^{-1} at $\sqrt{s} = 8$ TeV. Therefore, we concentrate on the ATLAS analysis.

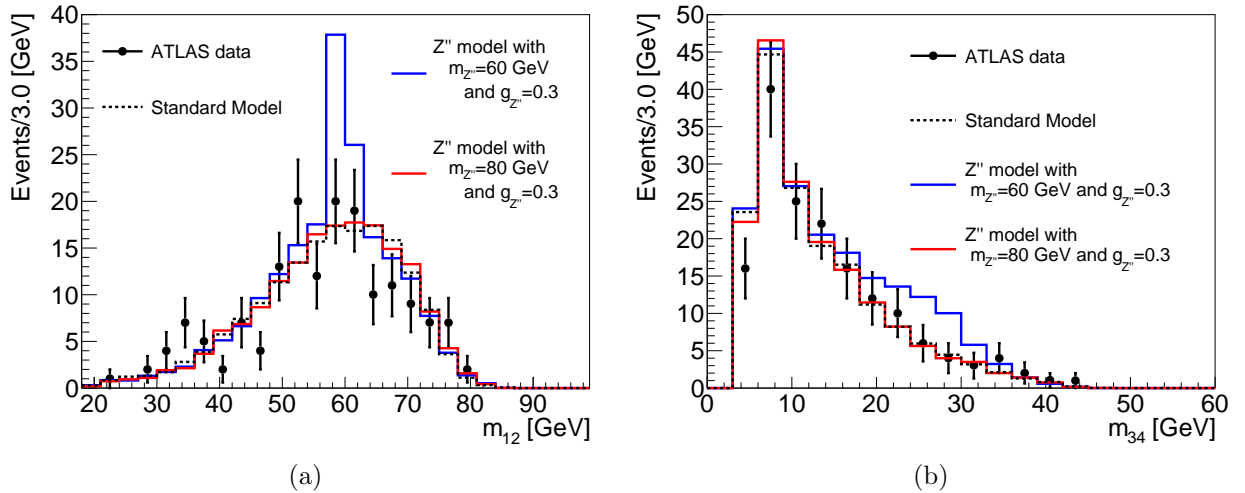


Figure 6: The m_{12} and m_{34} distributions for the SM (dashed) and for the Z'' models with $m_{Z''} = 60$ GeV (blue) and 80 GeV (red). All channels ($4e$, $2e2\mu$ and 4μ) are summed up. Combined results for the integrated luminosities of 4.6 fb^{-1} at $\sqrt{s} = 7$ TeV and 20.7 fb^{-1} at $\sqrt{s} = 8$ TeV are shown.

		N_{SM}	$N_{Z'',60}$	$\sigma_{Z'',60}$	$N_{Z'',80}$	$\sigma_{Z'',80}$
m_{12}	(51, 57) GeV	29.1	32.8	0.7	29.9	0.1
	(57, 63) GeV	34.2	63.9	5.1	35.1	0.2
	(63, 69) GeV	33.2	30.1	-0.5	32.3	-0.2
	(69, 75) GeV	20.7	19.5	-0.3	21.5	0.2
	(75, 81) GeV	4.7	5.2	0.2	5.9	0.5
m_{34}	(3, 18) GeV	130.6	135.2	0.4	131.8	0.1
	(18, 33) GeV	33.0	56.4	4.1	32.8	-0.0
	(33, 48) GeV	4.5	5.4	0.4	4.3	-0.1

Table 6: Event numbers in several m_{12} and m_{34} ranges. The luminosities of 4.6 fb^{-1} at $\sqrt{s} = 7 \text{ TeV}$ and 20.7 fb^{-1} at $\sqrt{s} = 8 \text{ TeV}$ are combined and event numbers in all channels ($4e$, $2e2\mu$ and 4μ) are summed up, as studied in Ref. [38]. N_{SM} and $N_{Z'',60}$ ($N_{Z'',80}$) are numbers of events in the SM and the Z'' model with $m_{Z''} = 60 \text{ GeV}$ (80 GeV), respectively. We also show the significance $\sigma_{Z''} = (N_{Z''} - N_{\text{SM}})/\sqrt{N_{\text{SM}}}$.

In the following we compare our simulation results with the ATLAS results. In order to adjust K -factor, acceptance and efficiency factors in the simulation, we introduce a constant normalization factor in each of the channels ($4e$, $2e2\mu$ and 4μ) to match our LO SM results and the expected numbers of events in Table 4 in Ref. [38], which is obtained by NLO Monte Carlo program POWHEG[41] and data driven acceptance estimations. We use the same factors for the Z'' models.

In Figure 6 we show the di-lepton invariant mass m_{12} distributions and m_{34} distributions in the SM and Z'' models with $m_{Z''} = 60 \text{ GeV}$ (left panel) and 80 GeV (right panel). In this section, combined results for integrated luminosities of 4.6 fb^{-1} at $\sqrt{s} = 7 \text{ TeV}$ and for 20.7 fb^{-1} at $\sqrt{s} = 8 \text{ TeV}$ are shown. All channels ($4e$, $2e2\mu$ and 4μ) are summed up for these plots so that we can directly compare them with Figure 3(e) and 3(f) in Ref. [38].

For the Z'' model with $m_{Z''} = 60 \text{ GeV}$, a large excess should be seen around $m_{12} \simeq m_{Z''}$ in the m_{12} distribution. It is from the on-shell decay $Z \rightarrow Z''\ell^+\ell^-$ followed by $Z'' \rightarrow \ell^+\ell^-$. We also see a small excess around $m_{34} = 20 - 30 \text{ GeV}$ in the m_{34} distribution, and it corresponds to $m_Z - m_{Z''}$. On the other hand, we don't see significant deviations for $m_{Z''} = 80 \text{ GeV}$. Table 6 shows the expected numbers of events in several m_{12} and m_{34} ranges for the Z'' model with $m_{Z''} = 60 \text{ GeV}$ ($N_{Z'',60}$) and 80 GeV ($N_{Z'',80}$), and for the SM (N_{SM}). The “significance” value $\sigma_{Z''}$, which is defined by $(N_{Z''} - N_{\text{SM}})/\sqrt{N_{\text{SM}}}$ and represents the deviation from the SM, is also shown. For $m_{Z''} = 60 \text{ GeV}$, $\sigma_{Z'',60}$ values are about 5.1 and 4.1 in the range of $m_{12} = 57 - 63 \text{ GeV}$ and of $m_{34} = 18 - 33 \text{ GeV}$, respectively, and shows the clear deviation from the SM prediction, while $\sigma_{Z'',80}$ is smaller than 1 and not statistically significant.

We also compute the χ^2 values defined by

$$\chi^2 = \sum_i \left(\frac{N_{th}^i - N_{\text{DATA}}^i}{\sigma_i} \right)^2, \quad (4.12)$$

	SM	Z'' model ($m_{Z''} = 60$ GeV)	Z'' model ($m_{Z''} = 80$ GeV)
$\chi^2/(\text{d.o.f})$ in m_{12}	33.1/(19)	47.1/(19)	34.1/(19)
$\chi^2/(\text{d.o.f})$ in m_{34}	6.9/(14)	26.6/(14)	6.5/(14)

Table 7: χ^2 in the m_{12} and m_{34} distributions in the SM and the Z'' models with $m_{Z''} = 60$ and 80 GeV.

where N_{th}^i is the expected number of events in the i -th bin for the theoretical models (the SM and the Z'' models), N_{DATA}^i and σ_i are the number of events observed in the i -th bin for the data and the corresponding statistical error, respectively. The data are obtained from the ATLAS analysis [38].

Table 7 shows the χ^2 values for the m_{12} and m_{34} distributions for the SM and the Z'' models. We use 19 bins for the m_{12} distribution and 14 bins for the m_{34} distribution to calculate the χ^2 . Thus, the degree of freedom (d.o.f) of the χ^2 is 19 (14) for the m_{12} (m_{34}) distribution. We see that the χ^2 for the Z'' model with $m_{Z''} = 60$ GeV is much worse than those for the SM in both m_{12} and m_{34} distributions. The total of the $\chi^2/(\text{d.o.f})$ is 73.7/(33), and the probability to be the statistical fluctuation is 6.1×10^{-5} . The corresponding probability for the SM is 0.19.

From the m_{12} and m_{34} distributions, we conclude that the Z'' model with $m_{Z''} = 60$ GeV is excluded by the ATLAS analysis because the Z'' effects should have been clearly visible in the case. The case with different value of the coupling $g_{Z''}$ can be easily estimated in the same way. On the other hand, the χ^2 of the Z'' model with $m_{Z''} = 80$ GeV is almost the same as the one of the SM. The total χ^2 is $\chi^2/(\text{d.o.f}) = 40.6$, and the corresponding probability is 0.17. Thus, the current ATLAS analysis is not sensitive to the Z'' model with $m_{Z''} = 80$ GeV.

The difference between the SM and Z'' model would be more evident if one looks only at 4μ channel since the Z'' only couples to muons, although the ATLAS has not provided the separate results. In Table 8, the numbers of 4μ events expected in several m_{12} ranges for the SM and Z'' model with $m_{Z''} = 60$ GeV are listed. Compared with Table 6, $\sigma_{Z'',60}$ in the range $m_{12} = (57, 63)$ GeV is much larger.

4μ channel		N_{SM}	$N_{Z'',60}$	$\sigma_{Z'',60}$
m_{12}	(51, 57) GeV	13.4	17.1	1.0
	(57, 63) GeV	17.4	47.3	7.2
	(63, 69) GeV	17.5	14.1	-0.8

Table 8: Numbers of events in several m_{12} ranges in 4μ channel for the SM (N_{SM}) and Z'' model with $m_{Z''} = 60$ GeV ($N_{Z''}$). We also show $\sigma_{Z''} = (N_{Z''} - N_{\text{SM}})/\sqrt{N_{\text{SM}}}$.

For $m_{Z''} = 80$ GeV, the Z'' model is not constrained by the ATLAS analysis. In the case of $m_{Z''} \simeq m_Z$ or $m_{Z''} > m_Z$, the off-shell Z boson in the s -channel diagram as shown in Figure 5 is dominant in the signal events. That is the reason why the ATLAS measurement of the Z decays to 4 leptons is not sensitive for the heavier Z'' boson.

We can see this more clearly by the ratios of event numbers $N_{Z'',60}/N_{\text{SM}}$ and $N_{Z'',80}/N_{\text{SM}}$ in 4μ channel after the successive selection cuts shown in Table 9. The cuts 1 – 6 correspond to the ones summarized above. For the cut 1, additionally we require $m_{\mu^+\mu^-} > 4$ GeV for any combinations of opposite sign di-muons. The sensitivity to the signal increases as we apply more cuts in the Z'' model with $m_{Z''} = 60$ GeV while it decreases after the cut 6 in the Z'' model with $m_{Z''} = 80$ GeV. It is because the signal events for $m_{Z''} = 80$ GeV mostly come from the off-shell region of Z boson. Consequently, the ATLAS analysis is not directly sensitive to the heavier Z'' bosons.

In order to gain sensitivity for the heavier Z'' boson, we propose optimized selection cuts:

5' $m_{4l} > m_Z + 10$ GeV and reject the Higgs mass region, $|m_{4l} - m_h| > 10$ GeV.

6' $|m_{34} - m_Z| > 5$ GeV.

in addition to p_T , η and ΔR cuts (cuts 1 – 4). Since the signal events are mainly through s -channel off-shell Z boson, we reject the contributions through on-shell Z boson as well as on-shell Higgs boson by the first criteria (5'). The second criteria (6') is for rejecting ZZ production process, which is another SM background, where both m_{12} and m_{34} tend to be close to m_Z . On the other hand, in the Z'' signal events, m_{12} tends to be $m_{Z''}$, but m_{34} does not accumulate on any particular value. Therefore, it efficiently rejects the ZZ backgrounds while keeping most of the Z'' signal.

We show the m_{12} distributions in 4μ channel after applying these optimized cuts in Figure 7 for $m_{Z''} = 80, 90$, and 100 GeV. For all masses, excesses at $m_{12} = m_{Z''}$ are expected. Table 10 shows the expected numbers in several m_{12} ranges, the ratio $N_{Z''}/N_{\text{SM}}$, and the significance.

For $m_{Z''} = 80$ and 100 GeV, the $N_{Z''}/N_{\text{SM}}$ ratio is very high, 3.1 and 2.5, respectively. The number of event in the SM N_{SM} for $m_{12} \sim m_{Z''}$ is very small so that σ defined before does not express statistical significance. We estimate the statistical significance based on the Poisson distribution with the average number of events $N_{Z''}$ for the bin with $m_{Z''} - 3 \text{ GeV} < m_{12} <$

cut	$N_{Z'',60}/N_{\text{SM}}$	$N_{Z'',80}/N_{\text{SM}}$
1. 4μ events	1.21	1.02
2-3. $p_{T,\mu}$ and $\Delta R_{\mu,\mu}$ cut	1.26	1.04
4-5. $m_{\mu\mu}$ cuts	1.28	1.05
6. $m_{4\mu}$ in (80, 100) GeV	1.38	0.99

Table 9: Ratio of the event numbers in Z'' models divided by the SM one after the successive selection cuts discussed in the text.

$m_{Z''} + 3$ GeV. The probability p to have events number in the bin $N \leq N_{\text{SM}}^{\text{mode}}$ in the Poisson distribution with the average of $N_{Z''}$, where $N_{\text{SM}}^{\text{mode}}$ is the mode of the Poisson distribution with the average of N_{SM} , is 1.5×10^{-2} for $m_{Z''} = 80$ GeV (0.07 for $m_{Z''} = 100$ GeV). It is not enough to exclude the $m_{Z''} \geq 80$ GeV. ¶ Since $N_{Z''}/N_{\text{SM}}$ ratio is very large, the evidence of the Z'' should be obtained at 14TeV runs. We also checked the possibility to improve those significance by using the di-muon invariant mass closest to the hypothetical $m_{Z''}$ value instead of the m_{12} . However, it is not improved since it increases the SM background in the signal region as well.

For $m_{Z''} = 90$ GeV, we can see only a small excess over the SM Z boson peak in the m_{12} distribution in Figure 7 (b). The significance is less than 1 due to the overlapping large SM Z contributions.

4.2 4 lepton channels at $\sqrt{s} = 14$ TeV

In the previous section, we have shown that the heavy Z'' boson ($m_{Z''} > 80$ GeV) cannot be excluded by using the $\sqrt{s} = 7 - 8$ TeV run data of the LHC due to the limited integrated luminosities. In this section, we study the Z'' search at $\sqrt{s} = 14$ TeV with the integrated luminosity of 300 fb^{-1} and 3000 fb^{-1} for the same reference points defined in the previous subsection except the case with $m_{Z''} = 60$ GeV, which is already excluded. In this section, the leading order results without constant normalization factors are used for the cross sections. For the detector simulation, we adopt the trigger conditions for the run at $\sqrt{s} = 14$ TeV [39], as shown in Table 11 and implemented in Delphes. In addition to the 4μ channel discussed in the previous section, we also discuss the channels involving τ -leptons such as $2\mu 2\tau$ and 4τ since Z'' also couples to τ -leptons.

¶ On the other hand, p for $N \geq N_{Z''}^{\text{mode}}$ in the Poisson distribution with the average of N_{SM} is 4.7×10^{-3} for $m_{Z''} = 80$ GeV (0.096 for $m_{Z''} = 100$ GeV).

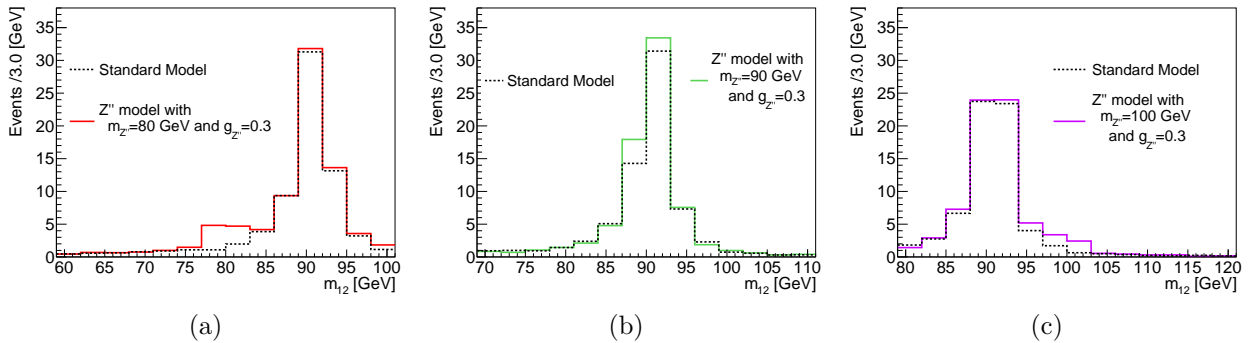


Figure 7: The distribution of the di-muon invariant mass m_{12} in $pp \rightarrow 4\mu$ in the SM (dashed line), Z'' model with $m_{Z''} = 80, 90$, and 100 GeV (solid lines, from left to right) after imposing the optimized cuts. Combined integrated luminosities of 4.6 fb^{-1} at $\sqrt{s} = 7$ TeV and 20.7 fb^{-1} at $\sqrt{s} = 8$ TeV are assumed.

$m_{Z''} = 80 \text{ GeV}$	N_{SM}	$N_{Z''}$	$N_{Z''}/N_{\text{SM}}$	prob. for $N < N_{\text{SM}}^{\text{mode}}$ in Z'' model
(71,77) GeV	2.0	2.5	1.2	–
m_{12} (77,83) GeV	3.1	9.5	3.1	1.5×10^{-2}
(83,89) GeV	13.2	13.5	1.0	–
$m_{Z''} = 90 \text{ GeV}$	N_{SM}	$N_{Z''}$	$N_{Z''}/N_{\text{SM}}$	$\sigma_{Z''}$
(81,87) GeV	7.5	6.9	0.9	–
m_{12} (87,93) GeV	45.7	51.4	1.1	0.9
(93,99) GeV	9.6	9.4	1.0	–
$m_{Z''} = 100 \text{ GeV}$	N_{SM}	$N_{Z''}$	$N_{Z''}/N_{\text{SM}}$	prob. for $N < N_{\text{SM}}^{\text{mode}}$ in Z'' model
(91,97) GeV	27.4	29.2	1.1	–
m_{12} (97,103) GeV	2.4	5.8	2.5	0.07
(103,109) GeV	0.9	1.0	1.1	–

Table 10: Numbers in several m_{12} ranges in 4μ channel after applying the optimized cuts in the SM and in the Z'' model for $m_{Z''} = 80, 90$, and 100 GeV . We assume combined integrated luminosities of 4.6 fb^{-1} at $\sqrt{s} = 7 \text{ TeV}$ and 20.7 fb^{-1} at $\sqrt{s} = 8 \text{ TeV}$.

trigger	p_T threshold
single muon	$p_T^\mu > 25 \text{ GeV}$
single tau jet	$p_T^\tau > 150 \text{ GeV}$
di-muon	$p_T^{\mu_1} > 13 \text{ GeV}, p_T^{\mu_2} > 13 \text{ GeV}$
muon-tau jet	$p_T^\mu > 15 \text{ GeV}, p_T^\tau > 40 \text{ GeV}$

Table 11: Trigger conditions relevant for the analysis at $\sqrt{s} = 14 \text{ TeV}$ [39].

4.2.1 $pp \rightarrow \mu^+ \mu^- \mu^+ \mu^-$

The excess of the Z'' signal which lies near Z boson mass in the m_{12} distribution would be confirmed at $\sqrt{s} = 14 \text{ TeV}$ since the cross section and number of events of the Z'' model would increase if Z'' boson exists for $pp \rightarrow 4\mu$ channels. We apply the optimized cuts for the heavier Z'' boson proposed in the previous section.

In Figure 8, we show the distributions of the di-muon invariant mass m_{12} for the SM and the Z'' model with $m_{Z''} = 80, 90$, and 100 GeV . We normalize the distributions for the integrated luminosity of 300 fb^{-1} . Excesses are more clearly seen in the Z'' model with $m_{Z''} = 80$ and 100 GeV in the signal region $m_{12} \simeq m_{Z''}$, compared with the case at $\sqrt{s} = 7-8 \text{ TeV}$. Even in the case of $m_{Z''} = 90 \text{ GeV}$, the excess in the region $m_{12} \simeq m_{Z''}$ is statistically significant. In Table 12, the numbers of events around the excesses for the SM (N_{SM}), for the Z'' models ($N_{Z''}$), the ratio $N_{Z''}/N_{\text{SM}}$ and $\sigma_{Z''}$ are shown. The significance $\sigma_{Z'',80}$ and $\sigma_{Z'',100}$ exceed 5. Although we obtain $\sigma_{Z'',90} \sim 3$ for $m_{Z''} = 90 \text{ GeV}$, whole region below $m_{Z''} \leq 100 \text{ GeV}$ will be explored at the high luminosity LHC (HL-LHC), where the expected integrated

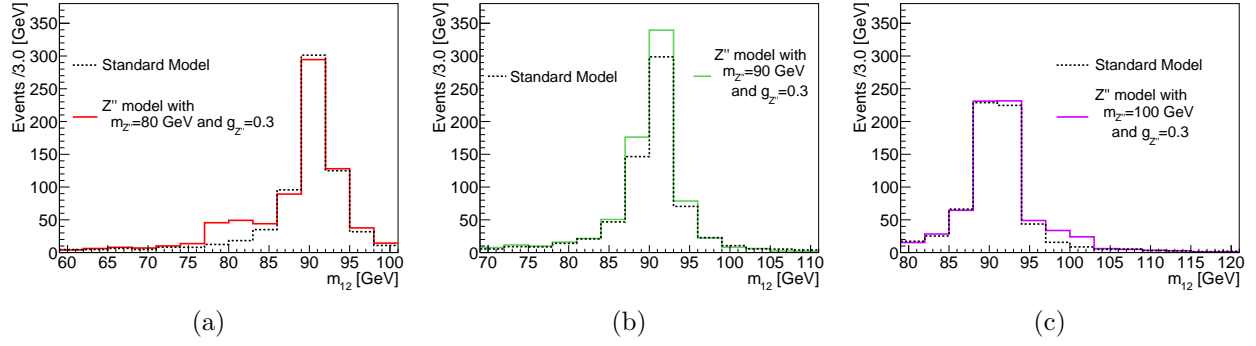


Figure 8: The m_{12} distributions in the 4μ channel in the SM (dashed line) and Z'' model with $m_{Z''} = 80, 90$, and 100 GeV (solid line, from left to right) after the optimized selection cuts. The integrated luminosity of 300 fb^{-1} at $\sqrt{s} = 14 \text{ TeV}$ is assumed.

$m_{Z''} = 80 \text{ GeV}$		N_{SM}	$N_{Z''}$	$N_{Z''}/N_{\text{SM}}$	$\sigma_{Z''}$
m_{12}	(71, 77) GeV	16.2	23.8	1.5	1.9
	(77, 83) GeV	30.7	94.7	3.1	11.6
	(83, 89) GeV	130.8	133.3	1.0	0.2
$m_{Z''} = 90 \text{ GeV}$		N_{SM}	$N_{Z''}$	$N_{Z''}/N_{\text{SM}}$	$\sigma_{Z''}$
m_{12}	(81, 87) GeV	67.6	72.1	1.1	0.5
	(87, 93) GeV	445.3	515.7	1.2	3.3
	(93, 99) GeV	93.3	100.9	1.1	0.8
$m_{Z''} = 100 \text{ GeV}$		N_{SM}	$N_{Z''}$	$N_{Z''}/N_{\text{SM}}$	$\sigma_{Z''}$
m_{12}	(91, 97) GeV	268.2	280.4	1.1	0.7
	(97, 103) GeV	24.3	57.8	2.4	6.8
	(103, 109) GeV	10.1	11.0	1.1	0.3

Table 12: Numbers of events in several m_{12} ranges in 4μ -channel at $\sqrt{s} = 14 \text{ TeV}$ with $\int dt L = 300 \text{ fb}^{-1}$ in the SM (N_{SM}) and in the Z'' model ($N_{Z''}$) with $m_{Z''} = 80, 90$, and 100 GeV after applying the optimized cuts.

luminosity is around $1000 - 3000 \text{ fb}^{-1}$, provided the cuts and background rate remain the same.

4.2.2 $pp \rightarrow \mu^+ \mu^- \tau^+ \tau^-$

In our Z'' model, the Z'' boson couples to the 2nd and 3rd generation leptons. In order to test the feature, we need to see the pattern of the couplings of the Z'' boson. One of these interesting processes is $2\mu 2\tau$ channel. To study this channel, we adopt hadronic τ tagging algorithm of Delphes which roughly reproduce ATLAS and CMS data for $Z \rightarrow \tau^+ \tau^-$ channel [36].

For this channel we require the following cuts:

1. two τ jets exist satisfying $p_{T,\tau} > 20$ GeV and $|\eta_\tau| < 2.3$, only hadronically decaying τ 's.
2. two oppositely charged muons exist satisfying $p_{T,\mu} > 10$ GeV and $|\eta_\mu| < 2.7$, the two muons are well separated as $\Delta R > 0.1$.
3. requiring the invariant mass cut for the two τ 's, $m_{\tau\tau} > 120$ GeV, where we adopt the collinear approximation for the τ momentum reconstruction, that is, the neutrino momentum from τ decay is assumed to be parallel to the τ jet direction.

The 1st and 2nd requirements select events which have 2μ and 2τ . The 3rd cut effectively rejects the SM ZZ backgrounds. It is because the signal matrix element is not enhanced at $m_{\tau\tau} \sim m_Z$ nor $m_{Z''}$ once we require $m_{\mu\mu} \sim m_{Z''}$. On the other hand, in the SM ZZ background both $m_{\mu\mu}$ and $m_{\tau\tau}$ are enhanced at m_Z . We found that the collinear approximation for the τ reconstruction is not good enough to reproduce the Z'' mass from the di-tau invariant mass. Nevertheless, we found it useful to reject the SM background.

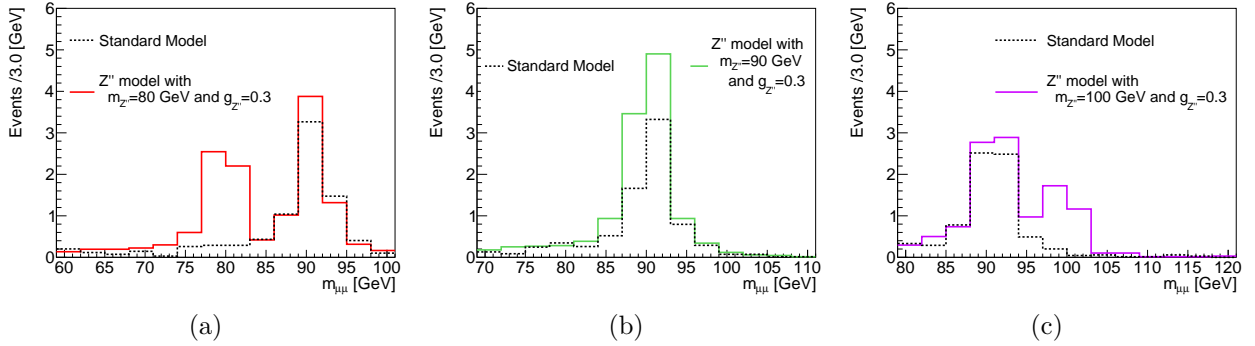


Figure 9: The $(m_{\mu\mu})$ distributions in the $2\mu 2\tau$ channel at $\sqrt{s} = 14$ TeV for the SM (dashed line) and for the Z'' model with $m_{Z''} = 80, 90$, and 100 GeV (solid lines, from left to right). The integrated luminosity of 300 fb^{-1} is assumed.

In 4μ channel there are two possible combinations to pair the muons. We have primarily used the m_{12} , which is the lepton pair closer to m_Z , for the Z'' boson search. By contrast, $2\mu 2\tau$ channel has no such combinatorial problem. In Figure 9, we show the di-muon invariant mass ($m_{\mu\mu}$) distributions for the SM (dashed line) and Z'' model with $m_{Z''} = 80, 90$, and 100 GeV (solid lines), from left to right panels, respectively. The normalizations are for the integrated luminosity of 300 fb^{-1} .

Table 13 shows event numbers in several $m_{\mu\mu}$ ranges around the excess for the Z'' models ($N_{Z''}$) together with those for the SM (N_{SM}), the ratio $N_{Z''}/N_{\text{SM}}$, and significance expressed by the required integrated luminosity for the discovery, which is defined as the integrated luminosity where the probability to have number of events in the signal bin $N > N_{Z''}$ is less than 10^{-5} for the Poisson distribution with the average of N_{SM} . The $N_{Z''}/N_{\text{SM}}$ is large

$m_{Z''} = 80 \text{ GeV}$	N_{SM}	$N_{Z''}$	$N_{Z''}/N_{\text{SM}}$	$\int dtL \text{ for discovery (fb}^{-1}\text{)}$
$m_{\mu\mu} \text{ (71, 77) GeV}$	0.3	0.9	3.1	> 500
$m_{\mu\mu} \text{ (77, 83) GeV}$	0.6	4.8	8.2	
$m_{\mu\mu} \text{ (83, 89) GeV}$	1.5	1.4	1.0	
$m_{Z''} = 90 \text{ GeV}$	N_{SM}	$N_{Z''}$	$N_{Z''}/N_{\text{SM}}$	$\int dtL \text{ for discovery (fb}^{-1}\text{)}$
$m_{\mu\mu} \text{ (81, 87) GeV}$	0.8	1.3	1.7	> 2900
$m_{\mu\mu} \text{ (87, 93) GeV}$	5.0	8.4	1.7	
$m_{\mu\mu} \text{ (93, 99) GeV}$	1.1	1.3	1.2	
$m_{Z''} = 100 \text{ GeV}$	N_{SM}	$N_{Z''}$	$N_{Z''}/N_{\text{SM}}$	$\int dtL \text{ for discovery (fb}^{-1}\text{)}$
$m_{\mu\mu} \text{ (91, 97) GeV}$	3.0	3.7	1.3	> 730
$m_{\mu\mu} \text{ (97, 103) GeV}$	0.3	2.9	11.8	
$m_{\mu\mu} \text{ (103, 109) GeV}$	0.07	0.2	2.9	

Table 13: Number of events in several $m_{\mu\mu}$ ranges in $2\mu 2\tau$ channel at $\sqrt{s} = 14 \text{ TeV}$ with $\int dtL = 300 \text{ fb}^{-1}$ in the SM and the Z'' model with $m_{Z''} = 80, 90$, and 100 GeV .

enough at $m_{\mu\mu} \sim m_{Z''}$ for both cases of $m_{Z''} = 80$ and 100 GeV , while it is only around 1.7 for $m_{Z''} = 90 \text{ GeV}$. The Z'' effects will be observed for $m_{Z''} = 80 \text{ GeV}$ with the luminosity less than 300 fb^{-1} . In the case of $m_{Z''} = 100 \text{ GeV}$ the number of signal events is small, but more data at the HL-LHC would strengthen the signal observation. In the case of $m_{Z''} = 90 \text{ GeV}$, the significance is smaller, however, it would be possible to observe the definite signal once we collect more data with the integrated luminosity of 3000 fb^{-1} at the HL-LHC assuming the acceptance of leptons and τ jets unchanged.

5 Conclusion

New particles with the mass of the order of the EW scale with a significant coupling to the muon sector can accommodate the muon g-2 anomaly. The LHC would be an important experiment to search such particles directly because of the high luminosity and cleanness of the muon signature.

In this paper, we have considered the $L_\mu - L_\tau$ gauge symmetry as one of the solutions to explain the anomaly of muon g-2. We have explicitly shown that the Z'' gauge boson of the EW scale mass explains the anomaly of muon g-2. We have also identified the parameter space where the Z'' model is consistent with the EW precision measurements. We have considered the LHC phenomenology for several reference model points in the preferred parameter space.

The Z'' model contribution to $Z \rightarrow 4\mu$ is large for the relatively light Z'' boson since a Z boson can decay into the Z'' boson. Therefore, we have closely checked the measurement of Z boson decay to 4 leptons ($4e$, 4μ , $2e2\mu$) at the ATLAS experiment. We conclude that the ATLAS result has already excluded the Z'' model with $m_{Z''} = 60 \text{ GeV}$ for $g_{Z''} = 0.3$. The ATLAS analysis is not sensitive yet to Z'' bosons with mass above $\sim 80 \text{ GeV}$. We have

proposed an analysis in $pp \rightarrow 4\mu$ channel sensitive to the heavier Z'' bosons, and have shown that the data at $\sqrt{s} = 7-8$ TeV should have some sensitivity to the Z'' boson with $m_{Z''} = 80$ and 100 GeV for $g_{Z''} = 0.3$.

Moreover, we have shown that LHC data at the 14 TeV LHC with 300 fb^{-1} would be enough to observe the clear Z'' boson signal in 4μ channel with $m_{Z''} = 80$ and 100 GeV for $g_{Z''} = 0.3$. Even in the case of $m_{Z''} = 90$ GeV, the integrated luminosity of 3000 fb^{-1} would reveal the Z'' model. Therefore, the current and future LHC data in the 4μ final state will provide the opportunity to explore the whole region of the Z'' model parameter space relevant to the muon g-2 anomaly.

In order to probe the Z'' model, we should observe the Z'' effects not only in the 4μ final state but also in the channels involving τ leptons such as the $2\mu 2\tau$ state since it is the important feature that the Z'' boson only couples to the 2nd and 3rd generation leptons. We have shown that the $Z''\tau^+\tau^-$ interaction would be probed in the $2\mu 2\tau$ final state with the LHC data of the integrated luminosity 3000 fb^{-1} at $\sqrt{s} = 14$ TeV for the preferable parameter region of the Z'' model. Future LHC data are crucial to test the new physics models responsible for the muon g-2 anomaly.

Acknowledgments

The authors acknowledge the Yukawa Institute for Theoretical Physics at Kyoto University, where this work was initiated during the YITP workshop “LHC vs Beyond the Standard Model –Frontier of particle physics (YITP-W-12-21)” held in March 19th-25th 2013 for hospitality, and they also thank participants of the workshop for the active discussions. The work is supported in part by a JSPS Research Fellowship for Young Scientists (K.H.), World Premier International Research Center Initiative (WPI Initiative), MEXT, Japan (K.H. and M.M.N.), and Grants-in-Aid for Scientific Research from the Ministry of Education, Science, Sports, and Culture (MEXT), Japan (No. 23104006 for M.M.N. and No. 22224003 for K.T.). MT wishes to thank the STFC for support from grant number ST/J002798/1 and Feng Luo for helpful discussions.

A Neutrino mixing and constraint from the washout of the baryon asymmetry

In this Appendix, we discuss the neutrino mixing in the $L_\mu - L_\tau$ gauged theory. We show that the observed neutrino mixing can be explained with an aid of three right-handed neutrinos. We also discuss the constraint from the washout of the baryon asymmetry in the early universe, and find that the masses of the right-handed neutrinos are bounded from above.

A.1 Neutrino mixing

In addition to the SM fields, we introduce three right-handed neutrinos $\nu_{iR} (i = e, \mu, \tau)$, in order to explain the observed neutrino mixing. We assume that they have $L_\mu - L_\tau$ charges of 0, +1, -1, respectively. We also assume that the $L_\mu - L_\tau$ gauge symmetry is broken by a condensation of a scalar field σ with a unit $L_\mu - L_\tau$ charge. The charge assignments of various fields are summarized in Table 14.

particle	L_1	L_2	L_3	$(e_R)^c$	$(\mu_R)^c$	$(\tau_R)^c$	$(\nu_{eR})^c$	$(\nu_{\mu R})^c$	$(\nu_{\tau R})^c$	σ	others
charge	0	+1	-1	0	-1	+1	0	-1	+1	+1	0

Table 14: Charges assignments under the $L_\mu - L_\tau$ gauge symmetry. All fermion fields are written in left-handed basis.

From the charge assignments, renormalizable terms in a Lagrangian which contribute to the lepton masses are given by

$$\begin{aligned} \mathcal{L} = & H^c (y_e L_1 (e_R)^c + y_\mu L_2 (\mu_R)^c + y_\tau L_3 (\tau_R)^c) + H (\lambda_1 L_1 (\nu_{eR})^c + \lambda_2 L_2 (\nu_{\mu R})^c + \lambda_3 L_3 (\nu_{\tau R})^c) \\ & + M_{ee} \nu_{eR} \nu_{eR} + M_{\mu\tau} \nu_{\mu R} \nu_{\tau R} + \lambda'_{e\mu} \sigma^\dagger \nu_{eR} \nu_{\mu R} + \lambda'_{e\tau} \sigma \nu_{eR} \nu_{\tau R} + \text{h.c.} \end{aligned} \quad (\text{A.1})$$

Here, y_e, y_μ, y_τ are the Yukawa couplings of the charged leptons and not related to the neutrino mass. The neutrino mass is determined from Yukawa couplings λ_i ($i = 1, 2, 3$), Majorana masses M_{ee} and $M_{\mu\tau}$, and Yukawa couplings $\lambda'_{e\mu}$ and $\lambda'_{e\tau}$.

Note that the mass terms between the left and right-handed neutrinos are diagonal. Therefore, the neutrino mixing is obtained by mixing among the right-handed neutrinos. If the Majorana masses $M_{ee}, M_{\mu\tau}, \lambda'_{e\mu} \langle \sigma \rangle$ and $\lambda'_{e\tau} \langle \sigma \rangle$ are of the same order, the seesaw mechanism [42] provides the observed order one neutrino mixing. From the seesaw formula, a relation between the parameters is given by

$$(\Delta m^2)^{1/2} \sim \frac{\lambda^2 v^2}{M} \sim 10^{-12} - 10^{-11} \text{ GeV}, \quad (\text{A.2})$$

where $v \simeq 174 \text{ GeV}$ is the vacuum expectation value of the SM Higgs, and Δm^2 is the difference between the mass squared of the left-handed neutrinos. λ and M denote λ_i ($i = 1, 2, 3$) and $M_{ee}, M_{\mu\tau}, \lambda'_{e\mu} \langle \sigma \rangle$ and $\lambda'_{e\tau} \langle \sigma \rangle$ collectively.

A.2 Washout of the baryon asymmetry

Interactions given by Eq. (A.1) break the lepton symmetry. On the other hand, $B + L$ symmetry is broken by the anomaly against the $SU(2)$ gauge interaction, whose effect is efficient at the early universe by the sphaleron process in the finite temperature [43]. Therefore, the baryon asymmetry is washed out if both effects are important simultaneously. Let us calculate a condition such that the washout does not occur.

First of all, the sphaleron process is efficient only at the temperature above the EW scale. Therefore, if the baryon asymmetry is generated below the EW scale, the washout does not occur. In the following, we assume that the baryon asymmetry is produced above the EW scale and calculate the constraint on the parameters in Eq. (A.1).

Let us consider two possibilities in which the washout does not occur.

1. λ_i is small,
2. M_{ee} and $M_{\mu\tau}$ are small.

If any of the two conditions are satisfied, the lepton number is effectively conserved. Therefore, one should adopt the weakest condition among them. Let us discuss the two cases in detail.

λ_i is small

In the limit $\lambda_i = 0$, the lepton symmetry is restored for each flavors. Therefore, if the interaction by λ_i is inefficient, the washout of the baryon asymmetry does not occur. The most efficient interaction is shown in Figure 10 and its rate is given by

$$\langle \sigma n v \rangle \simeq \frac{\lambda_i^2 y_t^2}{8\pi} T, \quad (\text{A.3})$$

where σ , n , v , y_t are the cross section of the process, the number density of related particles, the velocity of related particles, and the Yukawa coupling of the top quark, respectively. $\langle \cdots \rangle$ denotes the thermal average. By requiring that the rate is smaller than the Hubble scale for $T \gtrsim 10^2$ GeV, we obtain the bound

$$\lambda_i \lesssim 10^{-7}. \quad (\text{A.4})$$

M_{ee} and $M_{\mu\tau}$ are small

If both Majorana masses vanish, $L_e - L_\mu - L_\tau$ symmetry is restored. The most efficient interaction which induces the symmetry violation by the Majorana masses is shown in Figure 11. Its rate is given by

$$\langle \sigma n v \rangle \sim \frac{g'^4}{8\pi} M. \quad (\text{A.5})$$

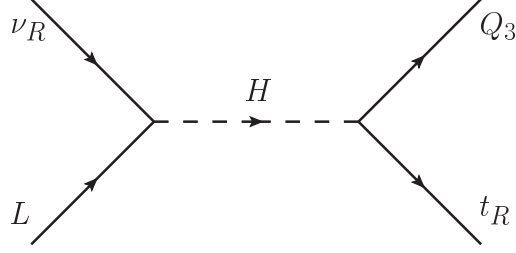


Figure 10: Feynman diagram for the lepton number violating interaction by λ .

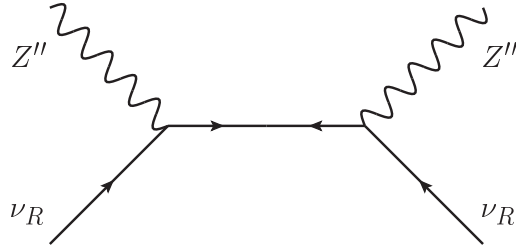


Figure 11: Feynman diagram for the lepton number violating interaction.

This rate is smaller than the Hubble scale for $T \gtrsim 10^2$ GeV if

$$M \lesssim 10^{-11} \text{ GeV} \left(\frac{g'}{0.3}\right)^{-4}. \quad (\text{A.6})$$

From the relation (A.2), one can see that the condition (A.6) is severer than the condition (A.4). Therefore, it is enough to satisfy the condition (A.4) in order for the washout not to occur. With the relation (A.2), the condition is interpreted as

$$\begin{aligned} \lambda_i &\lesssim 10^{-7} \\ M_{ee}, M_{\mu\tau} &\lesssim 10^1 \text{ GeV} \\ \lambda'_{e\mu}, \lambda'_{e\tau} &\lesssim 10^{-1} \frac{\langle\sigma\rangle}{100 \text{ GeV}} \end{aligned} \quad (\text{A.7})$$

Since the right-handed neutrinos are light and weakly coupled, it is necessary to consider whether they are long-lived. If they are long-lived, they might over-close the universe, or destroy the success of the big-bang nucleosynthesis (BBN). The most important decay channel is given by the diagram shown in Figure. 12. Here, we have assumed that σ is heavier than the right-handed neutrinos and hence the decay mode $N \rightarrow \sigma\nu$ is closed. The decay rate is given by

$$\Gamma \simeq \frac{M}{128\pi^3} \frac{M^2}{v^2} \lambda^2. \quad (\text{A.8})$$

The decay of the right-handed neutrinos is efficient around the temperature

$$T \sim 0.1 \text{ GeV} \frac{\lambda}{10^{-7}} \left(\frac{M}{10 \text{ GeV}}\right)^{3/2}. \quad (\text{A.9})$$

Therefore, the right-handed neutrinos decay before the BBN begins and does not affect it.

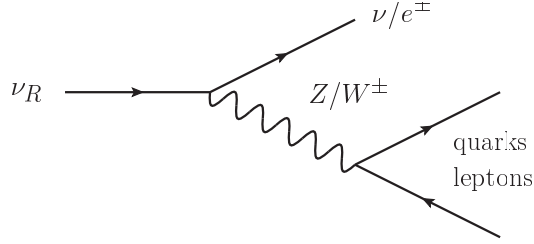


Figure 12: Feynman diagram for the decay of the right-handed neutrinos.

B Passarino-Veltman functions

Passarino-Veltman functions [44] are defined by

$$A(A) = 16\pi^2 \mu^{2\epsilon} \int \frac{d^n k}{i(2\pi)^n} \frac{1}{k^2 - m_A^2 + i\epsilon}, \quad (\text{B.10})$$

$$\begin{aligned} B_0(A, B; p) &= 16\pi^2 \mu^{2\epsilon} \int \frac{d^n k}{i(2\pi)^n} \frac{1}{[k^2 - m_A^2 + i\epsilon][(k+p)^2 - m_B^2 + i\epsilon]}, \\ p^\mu B_1(A, B; p) &= 16\pi^2 \mu^{2\epsilon} \int \frac{d^n k}{i(2\pi)^n} \frac{k^\mu}{[k^2 - m_A^2 + i\epsilon][(k+p)^2 - m_B^2 + i\epsilon]}, \\ p^\mu p^\nu B_{21}(A, B; p) &+ g^{\mu\nu} B_{22}(A, B; p) \\ &= 16\pi^2 \mu^{2\epsilon} \int \frac{d^n k}{i(2\pi)^n} \frac{k^\mu k^\nu}{[k^2 - m_A^2 + i\epsilon][(k+p)^2 - m_B^2 + i\epsilon]}, \end{aligned} \quad (\text{B.11})$$

$$\begin{aligned} &C_0(A, B, C; p_1, p_2) \\ &= 16\pi^2 \mu^{2\epsilon} \int \frac{d^n k}{i(2\pi)^n} \frac{1}{[k^2 - m_A^2 + i\epsilon][(k+p_1)^2 - m_B^2 + i\epsilon][(k+p_1+p_2)^2 - m_C^2 + i\epsilon]}, \\ &(p_1^\mu C_{11} + p_2^\mu C_{12})(A, B, C; p_1, p_2) \\ &= 16\pi^2 \mu^{2\epsilon} \int \frac{d^n k}{i(2\pi)^n} \frac{k^\mu}{[k^2 - m_A^2 + i\epsilon][(k+p_1)^2 - m_B^2 + i\epsilon][(k+p_1+p_2)^2 - m_C^2 + i\epsilon]}, \\ &\{(p_1^\mu p_1^\nu C_{21} + p_2^\mu p_2^\nu C_{22} + (p_1^\mu p_2^\nu + p_1^\nu p_2^\mu) C_{23} + g^{\mu\nu} C_{24}\}(A, B, C; p_1, p_2) \\ &= 16\pi^2 \mu^{2\epsilon} \int \frac{d^n k}{i(2\pi)^n} \frac{k^\mu k^\nu}{[k^2 - m_A^2 + i\epsilon][(k+p_1)^2 - m_B^2 + i\epsilon][(k+p_1+p_2)^2 - m_C^2 + i\epsilon]}, \end{aligned} \quad (\text{B.12})$$

where we use dimensional regularization in $4 - 2\epsilon$ dimensions, and μ is a renormalization scale.

We list some explicit expressions in the following, where $\frac{1}{\Delta} = \frac{1}{\epsilon} - \gamma + \log 4\pi$:

$$A(m^2) = m^2 \left(\frac{1}{\Delta} + 1 - \log \frac{m^2}{\mu^2} \right), \quad (\text{B.13})$$

$$B_0(A, B; p) = \frac{1}{\Delta} - \int_0^1 dx \log \frac{m_A^2(1-x) + m_B^2 x - p^2 x(1-x) - i\epsilon}{\mu^2}, \quad (\text{B.14})$$

$$B_1(A, B; p) = -\frac{1}{2\Delta} + \int_0^1 dx x \log \frac{m_A^2(1-x) + m_B^2 x - p^2 x(1-x) - i\epsilon}{\mu^2}, \quad (\text{B.15})$$

$$B_{21}(A, B; p) = \frac{1}{3\Delta} - \int_0^1 dx x^2 \log \frac{m_A^2(1-x) + m_B^2 x - p^2 x(1-x) - i\epsilon}{\mu^2}, \quad (\text{B.16})$$

$$B_{22}(A, B; p) = \frac{1}{4}(m_A^2 + m_B^2 - \frac{p^2}{3}) \left(\frac{1}{\Delta} + 1 \right) - \frac{1}{2} \int_0^1 dx \{ m_A^2(1-x) + m_B^2 x - p^2 x(1-x) \} \log \frac{m_A^2(1-x) + m_B^2 x - p^2 x(1-x) - i\epsilon}{\mu^2} \quad (\text{B.17})$$

References

- [1] G. Aad *et al.* [ATLAS Collaboration], Phys. Lett. B **716**, 1 (2012).
- [2] S. Chatrchyan *et al.* [CMS Collaboration], Phys. Lett. B **716**, 30 (2012).
- [3] J. Beringer *et al.* [Particle Data Group Collaboration], Phys. Rev. D **86**, 010001 (2012) and 2013 partial update for the 2014 edition.
- [4] T. Aoyama, M. Hayakawa, T. Kinoshita and M. Nio, Phys. Rev. Lett. **109**, 111808 (2012) [arXiv:1205.5370 [hep-ph]].
- [5] A. Czarnecki, W. J. Marciano and A. Vainshtein, Phys. Rev. D **67**, 073006 (2003) [Erratum-ibid. D **73**, 119901 (2006)].
- [6] K. Hagiwara, R. Liao, A. D. Martin, D. Nomura and T. Teubner, J. Phys. G **38**, 085003 (2011) [arXiv:1105.3149 [hep-ph]].
- [7] T. Teubner, K. Hagiwara, R. Liao, A. D. Martin and D. Nomura, Chin. Phys. C **34**, 728 (2010) [arXiv:1001.5401 [hep-ph]].
- [8] M. Benayoun, P. David, L. DelBuono and F. Jegerlehner, Eur. Phys. J. C **72**, 1848 (2012) [arXiv:1106.1315 [hep-ph]].
- [9] F. Jegerlehner and R. Szafron, Eur. Phys. J. C **71**, 1632 (2011) [arXiv:1101.2872 [hep-ph]].
- [10] F. Jegerlehner and A. Nyffeler, Phys. Rept. **477**, 1 (2009) [arXiv:0902.3360 [hep-ph]].

- [11] M. Davier, A. Hoecker, B. Malaescu and Z. Zhang, Eur. Phys. J. C **71**, 1515 (2011) [Erratum-ibid. C **72**, 1874 (2012)].
- [12] T. Moroi, Phys. Rev. D **53**, 6565 (1996) [Erratum-ibid. D **56**, 4424 (1997)].
- [13] For example, see T. Hambye, K. Kannike, E. Ma and M. Raidal, Phys. Rev. D **75**, 095003 (2007) [hep-ph/0609228]; S. Kanemitsu and K. Tobe, Phys. Rev. D **86**, 095025 (2012) [arXiv:1207.1313 [hep-ph]].
- [14] G. Abbiendi *et al.* [OPAL Collaboration], Eur. Phys. J. C **33**, 173 (2004) [hep-ex/0309053].
- [15] J. Abdallah *et al.* [DELPHI Collaboration], Eur. Phys. J. C **45**, 589 (2006) [hep-ex/0512012].
- [16] T. Aaltonen *et al.* [CDF Collaboration], Phys. Rev. Lett. **102**, 091805 (2009) [arXiv:0811.0053 [hep-ex]].
- [17] V. M. Abazov *et al.* [D0 Collaboration], Phys. Lett. B **695**, 88 (2011).
- [18] G. Aad *et al.* [ATLAS Collaboration], JHEP **1211**, 138 (2012) [arXiv:1209.2535 [hep-ex]].
- [19] S. Chatrchyan *et al.* [CMS Collaboration], Phys. Lett. B **720**, 63 (2013) [arXiv:1212.6175 [hep-ex]].
- [20] P. Fayet, Phys. Rev. D **75**, 115017 (2007) [hep-ph/0702176 [HEP-PH]].
- [21] M. Pospelov, Phys. Rev. D **80**, 095002 (2009) [arXiv:0811.1030 [hep-ph]].
- [22] M. Endo, K. Hamaguchi and G. Mishima, Phys. Rev. D **86**, 095029 (2012) [arXiv:1209.2558 [hep-ph]].
- [23] H. Davoudiasl, H. -S. Lee and W. J. Marciano, Phys. Rev. D **86**, 095009 (2012) [arXiv:1208.2973 [hep-ph]].
- [24] X. -G. He, G. C. Joshi, H. Lew and R. R. Volkas, Phys. Rev. D **44**, 2118 (1991).
- [25] S. Baek, N. G. Deshpande, X. G. He and P. Ko, Phys. Rev. D **64**, 055006 (2001) [hep-ph/0104141].
- [26] E. Ma, D. P. Roy and S. Roy, Phys. Lett. B **525**, 101 (2002) [hep-ph/0110146].
- [27] E. Salvioni, A. Strumia, G. Villadoro and F. Zwirner, JHEP **1003**, 010 (2010).
- [28] J. Heeck and W. Rodejohann, Phys. Rev. D **84**, 075007 (2011) [arXiv:1107.5238 [hep-ph]].

- [29] C. D. Carone and H. Murayama, Phys. Rev. Lett. **74**, 3122 (1995) [hep-ph/9411256]; Phys. Rev. **D52**, 484 (1995) [hep-ph/9504393].
- [30] G. -C. Cho *et al.*, JHEP **1111**, 068 (2011) [arXiv:1104.1769].
- [31] G. -C. Cho and K. Hagiwara, Nucl. Phys. B **574**, 623 (2000) [hep-ph/9912260].
- [32] K. Hagiwara *et al.*, Z. Phys. C **64**, 559 (1994) [Erratum-ibid. C **68**, 352 (1995)] [hep-ph/9409380].
- [33] S. Schael *et al.* [ALEPH and DELPHI and L3 and OPAL and SLD and LEP Electroweak Working Group and SLD Electroweak Group and SLD Heavy Flavour Group Collaborations], Phys. Rept. **427**, 257 (2006) [hep-ex/0509008].
- [34] A. Belyaev, N. D. Christensen and A. Pukhov, Comput. Phys. Commun. **184**, 1729 (2013) [arXiv:1207.6082 [hep-ph]].
- [35] T. Sjostrand, S. Mrenna and P. Z. Skands, JHEP **0605**, 026 (2006) [hep-ph/0603175].
- [36] S. Olyn, X. Rouby and V. Lemaitre, arXiv:0903.2225 [hep-ph].
- [37] S. Chatrchyan *et al.* [CMS Collaboration], JHEP **1212**, 034 (2012) [arXiv:1210.3844 [hep-ex]].
- [38] ATLAS Collaboration, “ATLAS measurements of the 7 and 8 TeV cross sections for $Z \rightarrow 4l$ in pp collisions”, ATLAS-CONF-2013-055 (May 27, 2013).
- [39] K. Nakamura, talk at “Summer camp on ILC accelerator and physics/detectors 2013”, Toyama, Japan, July 2013.
- [40] ATLAS Collaboration, ATLAS-CONF-2013-013.
- [41] P. Nason, JHEP **0411**, 040 (2004); S. Frixione, P. Nason and C. Oleari, JHEP **0711**, 070 (2007); S. Alioli, P. Nason, C. Oleari and E. Re, JHEP **1006**, 043 (2010); T. Melia, P. Nason, R. Rontsch and G. Zanderighi, JHEP **1111**, 078 (2011).
- [42] T. Yanagida, in “Proceedings of the Workshop on Unified Theory and Baryon Number of the Universe,” eds; O. Sawada and A. Sugamoto (KEK, 1979) p.95; M. Gell- Mann, P. Ramond and R. Slansky, in “Supergravity,” eds.; P. van Nieuwenhuizen and D. Freedman (North Holland, Amsterdam, 1979). See also P. Minkowski, Phys. Lett. **B67**, 421 (1977).
- [43] V. A. Kuzmin, V. A. Rubakov and M. E. Shaposhnikov, Phys. Lett. B **155**, 36 (1985).
- [44] G. 't Hooft and M. J. G. Veltman, Nucl. Phys. B **153**, 365 (1979); G. Passarino and M. J. G. Veltman, Nucl. Phys. B **160**, 151 (1979).